The Journal of Experimental Biology 213, 1060-1068

doi:10.1242/jeb.034678

Neuromechanical simulation of the locust jump

D. Cofer[1], G. Cymbalyuk[2], W. J. Heitler[4] and D. H. Edwards[3,*]

[1]Departments of Biology, [2]Physics and Astronomy and [3]Neuroscience Institute, Georgia State University, Atlanta, GA 30303, USA and [4]School of Biology, University of St Andrews, St Andrews, Fife, KY16 9TS, UK

*Author for correspondence (dedwards@gsu.edu)

Accepted 29 November 2009

SUMMARY

The neural circuitry and biomechanics of kicking in locusts have been studied to understand their roles in the control of both kicking and jumping. It has been hypothesized that the same neural circuit and biomechanics governed both behaviors but this hypothesis was not testable with current technology. We built a neuromechanical model to test this and to gain a better understanding of the role of the semi-lunar process (SLP) in jump dynamics. The jumping and kicking behaviors of the model were tested by comparing them with a variety of published data, and were found to reproduce the results from live animals. This confirmed that the kick neural circuitry can produce the jump behavior. The SLP is a set of highly sclerotized bands of cuticle that can be bent to store energy for use during kicking and jumping. It has not been possible to directly test the effects of the SLP on jump performance because it is an integral part of the joint, and attempts to remove its influence prevent the locust from being able to jump. Simulations demonstrated that the SLP can significantly increase jump distance, power, total energy and duration of the jump impulse. In addition, the geometry of the joint enables the SLP force to assist leg flexion when the leg is flexed, and to assist extension once the leg has begun to extend.

Supplementary material available online at http://jeb.biologists.org/cgi/content/full/213/7/1060/DC1

Key words: locust, semi-lunar process, jumping, kicking, biomechanics, Hill muscle model, muscle, neuromechanical simulation, model, neural circuit, invertebrate.

INTRODUCTION

The ability to escape predators is of great evolutionary importance. Many animals, including the locust, have evolved to specialize in jumping as a method of escape and locomotion. The locust jump is mediated by neural and biomechanical mechanisms that first prepare the animal for the jump by storing mechanical energy in the legs, and then release it suddenly to catapault the animal into the air. Because of the impossibility of making the necessary measurements during a jump, the mechanisms have primarily been studied during a different behavior, the kick, when the locust body is held stationary (Heitler, 1988; Heitler and Burrows, 1977a; Heitler and Burrows, 1977b). The kick and the jump both involve rapid extension of the leg, but because the kick is unloaded, it occurs much more rapidly than the jump. Despite this difference, the similar neuromuscular activity before and during both behaviors has led to the suggestion that the kick and jump motor programs are the same (Heitler and Burrows, 1977a).

The locust kick/jump motor program consists of three phases (Burrows, 1995; Heitler and Burrows, 1977a). The first phase is cocking the leg. The locust prepares for a jump by activating the flexor tibia muscle to bring the tibia into a fully flexed position. The second phase is a period of co-contraction where both the extensor and flexor tibia muscles are active. The extensor tibia muscle slowly contracts and stores energy in the extensor apodeme, in the semi-lunar process (SLP) and in the leg cuticle. As tension builds in the flexor tibia, its distal tendon passes over a cuticular invagination in the ventral aspect of the distal ventral femur called Heitler's lump (Bennet-Clark, 1975). This enables the flexor tibia tendon to attach to the tibia at an angle of nearly 90 deg. when the tibia is fully flexed, thereby maximizing its mechanical effectiveness in maintaining tibial flexion against the increasing tension in the much larger extensor tibia muscle (Heitler, 1974). The lump also acts as a catch or lock on the tendon that helps keep the tibia flexed while the flexor muscle has tension. In the third phase, the jump is triggered when both the flexor muscle and its motor neurons are inhibited. When the flexor tension drops below a threshold, the tendon slips off the catch and the tibia is rapidly extended to produce the jump (Heitler, 1974).

Technical limitations have prevented a clear understanding of the role of the SLP in the kick and jump. The SLP is a highly sclerotized portion of cuticle at the femoral–tibia joint of the metathoracic leg. In preparation for a kick or jump, the SLP bends like an archery bow during a slow contraction of the powerful extensor muscle to store energy that is later released rapidly to power the kick or jump (Bennet-Clark, 1975). The function of the SLP has been inferred from its movement during kicks as recorded by high-speed video and from calculations of the energy stored in the extensor apodeme, the SLP and the femur cuticle (Bennet-Clark, 1975; Burrows and Morris, 2001). The energy stored in the SLP and the timing of its release appear to be important for jump performance. High-speed video of locusts kicks show that the SLP does not begin unfurling until the tibia has rotated by more than 30 deg. (Burrows and Morris, 2001). The reason for this delay and the role it may play in the jump dynamics are unknown. Damage to the SLP, which is an integral part of the leg joint, makes the locust unable to jump, and so makes comparisons of the jump performance of animals with and without a functional SLP almost impossible.

The emerging field of neuromechanical simulation can help address these issues (Pearson et al., 2006). We have used a new neuromechanical simulator, AnimatLab (www.animatlab.com), to build and test a model of the locust based on current descriptions of the neural and biomechanical processes that govern the jump.

The model locust was then situated in a physically realistic environment within AnimatLab to study both the ability of the kick motor program to produce a realistic jump and the effects of the SLP on jumping behavior.

MATERIALS AND METHODS

Animals

Adult locusts, *Schistocerca americana* L., were obtained from a breeding colony at Agnes Scott College, Decatur, GA, USA, kept caged in small groups at 27°C under a 12 h:12 h L:D cycle, and fed fresh organic lettuce and 2/1 mixture of fresh wheat germ and powdered milk. Individuals were taken from the cage to a video-recording room and placed on a jumping platform. The platform contained a heating element that could adjust the local temperature and was covered by very fine sandpaper to allow the locust a slip-free surface for jumping. A 25 cm × 30 cm yellow wooden target was placed 30 cm from the platform, and jumps to the target were induced by either gentle touches of the abdomen by a hand-held wand or by raising the temperature of the platform. Animals were retrieved after the jump and returned to the platform for another attempt. Jumps were evoked at about 5 min intervals; individuals were returned to their cage after 10 jumps. Locust jumps were recorded at 500 frames s^{-1} and a resolution of 512 pixels × 240 pixels by two Photron PIC R2 Fastcam video cameras (San Diego, CA, USA) with an exposure time of 0.5 ms.

Locust model

To distinguish references to the model and its parts from references to the locust, the model part names have been given the italicized names of the corresponding locust body parts whereas references to the locust and its body parts are made in normal font.

The 3-D graphical model of the *locust body* was developed from a 3-D polygon mesh that was purchased online (www.turbosquid.com) and then separated into individual *body segments* using the graphics program Blender (www.blender.org). A polygon mesh is a set of vertices and triangular faces that define the volume for that segment. The dimensions of each *segment* were re-scaled to match published anatomical measurements (Bennet-Clark, 1975; Heitler, 1974). All *segments* were assumed to have a uniform density, and the distribution of mass throughout the mesh volume determined the moment of inertia for that *segment*. The model has a body length of 48 mm and a total mass of 2.5 g, with *metathoracic femur* and *tibia* lengths of 26 mm (Bennet-Clark, 1975). Individual body and limb *segments* were connected with either static or planar hinge joints in AnimatLab to assemble the locust body model. Angular limits on the hinge joints were set to restrict the movement of each joint to the normal range of the corresponding animal's joint. To ensure that the center of mass (COM) of the whole *locust* was located appropriately, small weighted masses were placed along the *body* axis of the *thorax* and *abdominal segments* to adjust the distribution of mass within the *body* (Bennet-Clark, 1975). The COM was then determined by pinning the *body* to a hinge joint and allowing it to rotate freely. Mass was re-distributed until the *locust* balanced both vertically and horizontally at the desired location. The locust model used for these simulations can be found at www.animatlab.com/locust.

Biomechanics

The geometry and biomechanical properties of the femur–tibia joint of the metathoracic leg play a crucial role in the energy storage for the jump (Fig. 1). The *tibia extensor muscle/apodeme* is shown as a red line that attaches to the *tibia* (Fig. 1a) whereas the *tibia flexor muscle/apodeme* is shown in green. It wraps over *Heitler's lump* (Fig. 1h) and attaches to the *tibia* (Fig. 1c). The *femur* was connected to a small block of mass 1.6 mg that represented the *SLP* (Fig. 1f) (Bennet-Clark, 1975). A sliding prismatic joint connected the *SLP* to the *femur* (Fig. 1g). During normal co-contraction, the distal end of the SLP (where the tibia attaches) moves 0.3 mm ventrally and 0.4 mm proximally (Burrows and Morris, 2001). The slider joint was oriented to allow the *SLP* mass to move in the same direction (Fig. 1b–g). A spring attached the *SLP* mass to the *femur* and was oriented along the direction of movement of the slider joint (Fig. 1e). The stiffness of the semi-lunar spring was calculated from a stress–strain curve obtained for the SLP (Bennet-Clark, 1975). Straining the process parallel to the extensor apodeme by 0.4 mm required approximately 14.2 N of force (Bennet-Clark, 1975). However, the SLP moves both proximally and ventrally, and this amount of proximal strain corresponds to 0.3 mm of ventral strain, for 0.5 mm of total strain. From this strain, we calculated the stiffness of the SLP as 28.4 kN m^{-1}. The *semi-lunar* spring constant was set to this value.

The *tibia* was connected to the *SLP* mass by a hinge joint that allowed the *tibia* to rotate between 5 deg. and 160 deg. (Fig. 1b). The *femur–tibia* hinge joint is connected to the SLP mass, so that during co-contraction and *tibial* extension, the hinge joint will move

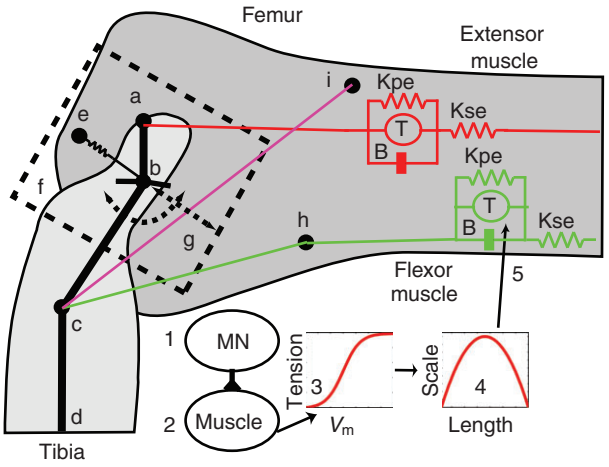

Fig. 1. Model of the *femur–tibia* (*FT*) joint of the *metathoracic leg*. (a) *Extensor apodeme* attachment point on the *tibia*. (b) *FT hinge joint* and connection of *semi-lunar process* (*SLP*) spring. (c) *Flexor apodeme attachment* point on the *tibia*. (d) A more distal point on the tibia. (e) The *SLP* spring is attached between the *femur* and the *tibia*. (f) The *SLP mass* moves along the slider joint (g) oriented between the points b and g that is at an inclination of 36.9 deg. (h) *Heitler's lump*. The *flexor muscle* wraps over this lump to alter its orientation with respect to the *tibia* as the *leg* is moved. (i) The *tendon lock* is modeled as a spring located between points c and i (magenta line). It is only enabled when the *tibia* is fully flexed and *flexor muscle* has a tension greater than 0.15 N (Bennet-Clark, 1975; Heitler, 1974). The distance between a,b is 0.76 mm, b,c is 1.64 mm. The angle a,b,c is 144 deg. and b,c,d is 143 deg. (Heitler, 1974). The muscle model is shown for the flexor and extensor muscles. This consists of a spring (*K*pe), in parallel with a tension generator (T), and a dashpot (B), in series with another spring (*K*se). (1) The muscle is activated by firing of a motor neuron (MN). (2) This depolarizes the muscle membrane. (3) Changes in the membrane voltage (V_m) are converted to a tension value using a sigmoidal function. (4) The tension value is scaled based on the muscle length. (5) The scaled tension is applied to the muscle by the force generator to produce a contraction. *Tibia extensor muscle/apodeme* is shown as a red line, and the *tibia flexor muscle/apodeme* is shown in green.

along the slider with the *SLP* mass to approximate the joint movement observed in the locust (Burrows and Morris, 2001). The distances and angles that define the relationships between the *extensor* attachment, *femur–tibia* hinge joint and *flexor* attachment were set to published measured values (the distance between a,b is 0.76 mm and between b,c is 1.64 mm. The angle a,b,c is 144 deg. and the angle b,c,d is 143 deg.) (Heitler, 1974).

Muscle is represented in AnimatLab by a linear Hill muscle model (Hill, 1970; McMahon, 1984; Shadmehr and Wise, 2005a; Shadmehr and Wise, 2005b). Each muscle model consists of a serial spring (Kse) in series with the parallel combination of a parallel spring (Kpe), a dashpot (B) and a force actuator (T). Muscle model properties are determined by the resting muscle length, the spring and dashpot constants, the stimulus–tension curve and the length–tension curve. The stimulus–tension curve is a sigmoidal function that relates the force level of the actuator to muscle membrane depolarization. The length–tension curve is an inverse parabola that determines the percentage of actuator force that is applied at a given muscle length.

Only two muscles for each of the rear legs are modeled in this simulation, the flexor tibiae and extensor tibiae. The maximum force that can be produced by the extensor is 15 N, which is achieved upon depolarization after a latency of 300–800 ms (Bennet-Clark, 1975). The serial spring constant of the *extensor* was calculated using the Young's modulus of 18.9 kN mm^{-2} found for the extensor apodeme by Bennet-Clark (Bennet-Clark, 1975). The average size of the apodeme test pieces was 3 mm long × 0.25 mm wide × 40 μm thick, and so they have an area of 0.01 mm^2, and a length of 3 mm. These values allowed us to calculate the spring constant as 63 kN m^{-1} from Young's modulus using the equation $K=YA/L$, where Y is the modulus, A is the area and L is the length. In the absence of published measurements that would allow calculation of the parallel spring constant, we used a value of 20 N m^{-1} because it produced a small but noticeable tension when the *extensor muscle* was stretched. The damping coefficient of the *extensor muscle* was set by hand to 700 Ns m^{-1} to produce a rise time to peak tension of approximately 400 ms. The stimulus–tension curve and the response properties of the non-spiking *neuron* that represents the muscle membrane were configured to reproduce the twitch response of the extensor muscle to a single *FETi* spike at a femur–tibia angle of 90 deg. (Heitler, 1988). The length–tension curve was also reproduced from muscle twitch values that were taken at various femur–tibia angles by stimulation of the muscle (Bennet-Clark, 1975). Stimulation of the *extensor muscle* produced twitch responses very similar to those recorded from extensor muscle in response to a FETi spike. The resulting length–tension curve of the *extensor muscle* reached the maximum at the fully flexed position and was reduced as the *leg* extended.

Recordings from the flexor muscle showed that it produces a maximum tension of around 0.75 N in response to tetanizing stimulation, and that it reached maximum tension 35–40 ms after a latency of 15 ms (Bennet-Clark, 1975). The following parameter values enabled the *flexor muscle* model to reproduce the recorded peak tension and tension time course; the serial spring constant, K_{se}, was 100 N m^{-1}, the parallel spring constant K_{pe} was 20 N m^{-1} and the damping coefficient, B, was 10 Ns m^{-1}. The stimulus–tension curve was configured to produce the desired maximum tension. As with the *extensor* model, the *flexor* length–tension curve was near its maximum value when the *leg* was fully flexed and near its minimum value when the *leg* was extended.

The tendon on the flexor muscle of the locust contains a pocket. When the tibia is fully flexed and the flexor has a tension greater than 0.15 N, this pocket is caught on Heitler's lump, which helps keep the tendon locked in place (Bennet-Clark, 1975; Heitler, 1974). This tendon lock property plays an important role in the jump after co-contraction when the flexor muscle and motor neurons are being inhibited. The lock helps keep the tibia fully flexed even while the flexor tension is dropping. This prevents premature extension of the tibia and initiates the jump once the flexor tension drops below a threshold value for maintaining the lock. In the model, the tendon lock was represented by a spring that connects the *flexor attachment* to a point on the *femur* (Fig. 1, magenta line between points c and i). The spring was disabled and produced no tension unless the *tibia* was fully flexed and the *flexor* tension was greater than 0.15 N.

Neural model

A conductance-based integrate-and-fire neuron model was used in this simulation. Neurons were modeled as single equipotential compartments, each characterized by a set of user-specifiable parameters, including membrane time-constant, size (i.e. input conductance), membrane voltage, current noise, initial spike threshold, spike-frequency accommodation, spike after-hyperpolarization conductance and calcium conductances with activation and inactivation variables (MacGregor and Lewis, 1977).

The neural network used to generate both the *kick and jump motor programs* was designed to apply the correct motor signals in a sequence and duration that mimics the motor program seen during kicking in locusts (Heitler and Burrows, 1977a; Heitler and Burrows, 1977b). Initial flexion of the *tibia* begins when the nine *fast flexor tibia motor neurons* are stimulated to fire (Fig. 2A, green *FLTi neurons*) (Burrows, 1995; Burrows, 1996). These neurons synapse onto the *flexor muscle membrane* (Fig. 2F, light blue *FM* node) causing *muscle* depolarization and *flexor muscle* contraction. The *fast extensor of the tibia motor neuron* (Fig. 2B, red *FETi neuron*) synapses onto the *extensor muscle membrane* (Fig. 2E, light blue *EM* node) causing it to contract. A central excitatory *synapse* connects the *FETi neuron* to the *fast flexor motor neurons* (B to A) (Burrows, 1996; Heitler and Burrows, 1977b). There are also two *inhibitory interneurons* that are involved in triggering the *jump*. The multimodal *'M' interneuron* (Fig. 2C, gold *M neuron*) inhibits the excitatory *flexor motor neurons*, while the inhibitory *flexor inhibitor motor neuron* (Fig. 2D, yellow *FI neuron*) *synapses* onto the *flexor muscle* and inhibits it directly (Burrows, 1995; Pearson et al., 1980). The *tendon lock control node* (Fig. 2G, light blue) is responsible for enabling the *tendon lock spring* when the *tibia* is sufficiently flexed and the *flexor* has a tension above the lock threshold. The network that governs the right *metathoracic leg* is shown in Fig. 2; an identical network governs the left *metathoracic leg*.

Neurons were configured to reproduce the observed firing frequencies during the kick. Peak *FETi* neuron firing ranged between 60 Hz and 100 Hz (Heitler and Burrows, 1977a), while the *FLTi* neurons fired around 60 Hz (Heitler and Burrows, 1977A). The central *excitatory synapse* connecting the *FETi* to the *FLTi neurons* was configured by reproducing an experiment in which the *FETi* was stimulated to fire at roughly 10 Hz while the *synaptic response* of the *FLTi* was monitored (Heitler and Burrows, 1977b). The first *FETi spike* produced a 20 mV *EPSP* (excitatory postsynaptic potential) in all of the *FLTi motorneurons*; the *EPSPs* decayed in approximately 100 ms (Burrows, 1996; Heitler and Burrows, 1977b). Responses to subsequent *spikes* were reduced by *synaptic depression* in a manner similar to that observed experimentally (Heitler and Burrows, 1977b).

All *neurons* had a random tonic noise of 0.3 mV added to their *membrane potentials* at each time step. The pseudo-random number

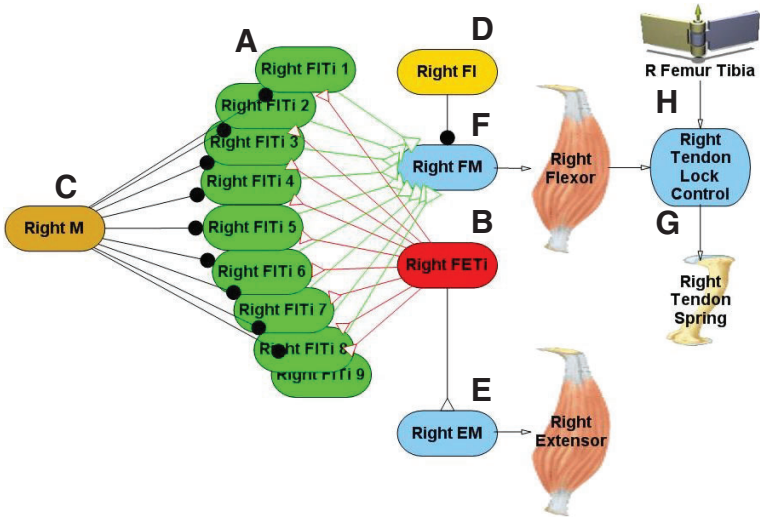

Fig. 2. Neural network model to produce the *kick* and *jump* motor programs. Network shown is for the right leg. (A) Nine *fast flexor tibia motor neurons* (green *FITi*). *FITi*s synapse onto the *flexor muscle* membrane (light blue *FM*). (B) A single *fast extensor tibia motor neuron* (red *FETi*). *FETi* synapses onto the *extensor muscle membrane* (light blue *EM*). (C) The *multimodal interneuron* (gold *M*) inhibits the *FITi*s. (D) The *flexor inhibitor* (yellow *FI*) inhibits the *flexor muscle*. (E) Depolarization of the *extensor muscle membrane* causes the *extensor muscle* to contract. (F) Depolarization of *the flexor muscle membrane* causes the *flexor muscle* to contract. (G) The *tendon lock* control node (light blue) controls when the *tendon lock spring* is enabled based on the rotation of the *tibia* and the tension in the *flexor muscle*. (H) When the *jump* is triggered the *femur–tibia* joint rotates rapidly to produce the *kick* or *jump*.

generator that controlled the noise was initialized using a random seed value at the beginning of each simulation. This caused each simulation with a different seed to produce slightly different results because changes in the *neuron* voltages led to alterations in the timing of the *motor program* and the rise and fall times of the tension in each of the *muscles*.

Procedures for simulation of experiments

During the *kick* simulations, the *locust* was suspended above the *ground* and rotated so that its *ventral surface* was uppermost, and pinned in place so it could not fall. All *leg joints* except the *femur–tibia* and *tibia–tarsus joints* of the *metathoracic legs* were locked to prevent rotation. The *kick motor program* caused the *tibia* to flex initially and then kick out at high speed. This allowed us to measure the movement of the *SLP* and *tibial* rotation. *SLP* torque relative to the *extensor attachment* was calculated by recording the coordinates of the *femur–tibia joint*, *extensor attachment* and the *SLP* force vector. These values were used to calculate the moment arm of the *SLP* force vector relative to the *extensor attachment*, and this was used to calculate the torque applied by the *SLP*. *Kick* velocity was measured as the peak velocity between the beginning of the *kick* and end of the *kick* when the *tibia* had fully rotated by 160 deg. *Kick* duration was the time from the beginning of the *kick* until full rotation of the *tibia*.

The same stimulus pattern that was used for *kicks* was applied to produce the motor pattern for the *jump*. Simulations of the locust jump began with the *locust* held 4.5 cm above the *ground*, and then dropped to the *ground*. Initially, only the *femur–tibia joints* of the *rear legs* were free to rotate. All of the other *joints* were locked and unmoving, and the rear *legs* were held up in the air to allow the *tibia* to rotate freely without interference with the *ground*. Once the *tibia* was fully flexed, the *metathoracic coax–femur joint* was adjusted to fix the angle of the *leg* with respect to the *ground* and ensure a take-off angle of approximately 55 deg. This angle was chosen because it produced *jumps* that minimized tumbling during take-off. The *joints* for all of the other *legs* remained locked throughout the *jump motor program* in order to maintain a stable and consistent posture, and the posture of the *front legs* was adjusted to fix the initial *body pitch* of the *animal* at 2 deg. The locks on the *joints* of the *front* and *middle legs* were disabled when the *jump* was triggered. This allowed all the *legs* to move freely throughout the take-off and ballistic phase of the *jump*. The *SLP* was disabled for tests by locking the *SLP* sliding prismatic joint to prevent it from moving and by disabling the *SLP* spring to prevent it from generating tension. Extensor tension was controlled by varying the firing frequency of the *FETi motor neurons*.

Predicted jump distance was calculated using the equation:

$$d = \frac{2 \cdot E \cdot \sin\left(2 \cdot \theta\right)}{m \cdot \boldsymbol{g}} \quad , \tag{1}$$

where d is distance, E is energy, θ is the average take-off angle for all simulated jumps, m is the mass and $\boldsymbol{g}$ is gravity (Bennet-Clark, 1975). The power of the *jump* was calculated as the dot product of the force acting on the *body* during the *jump* impulse and the velocity of the *body* (Bennet-Clark, 1975). The energy of the *jump* was calculated by integrating the power curve over the time period of the impulse. The beginning of a *jump* or *kick* was always measured from when the tendon lock was disengaged. *Jump* duration was the time from the beginning until either the *body* or one of the rear *legs* first touched the *ground*. *Jump* distance was measured as the difference between the positions of the *locust* at the end and at the beginning of the *jump*. *Jump* impulse duration was the time from the beginning of the *jump* until one of the *legs* lost contact with the *ground*. *Jump* velocity and acceleration was the peak of those values obtained during the *jump* impulse. All data analysis was performed in Matlab (Matlab R2007a, Mathworks Inc., Natick, MA, USA), and statistical comparisons were made using its Anova1 one-way analysis of variance function.

The influence of *SLP* flexion torque on the *flexor muscle* was determined by comparing the tension level at which the *extensor muscle* was able to overcome the tension in the *flexor* when the *SLP spring* was intact and when it was disabled. The *extensor* tension was set to 5 N, and the *tendon lock* was disabled for both tests. The first test was performed with the *SLP* intact whereas in the second test the *SLP spring* was disabled. Once the *extensor* reached the 5 N tension level the *flexor* was inhibited and its tension dropped until it reached a point where the *extensor muscle* was able to overcome it and extend the *leg*.

RESULTS

Motor program and jumping

The simulated motor program and patterns of *muscle* activity responsible for the *kick* are shown in Fig. 3. The *kick motor program* began by stimulating the nine *FlTi* motorneurons on the right and left side (Fig. 2) to fire at about 60 Hz, which produced tension in

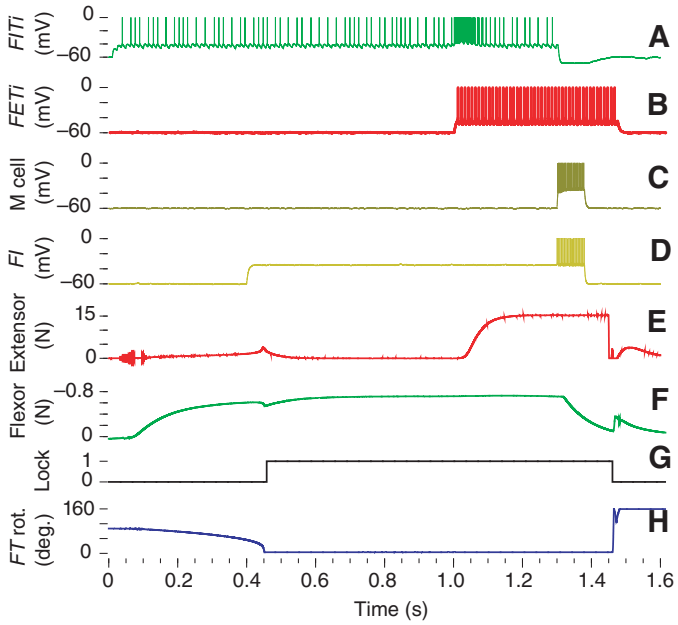

Fig. 3. Neural output of the jump motor network. The nine *flexor motor neurons* were stimulated to fire (A) during the cocking phase, which increased tension in the *flexor muscle* (F) and rotated the tibia into a fully flexed position (H). The *extensor motor neuron FETi* (B) began firing to produce co-contraction and increase *flexor* frequency through the central *excitatory synaptic connection* from *FETi to FLTi*. The *inhibitory interneurons M* (C) and *flexor inhibitor* (*FI*) (D) then began firing once the *extensor* had reached the desired tension level (E). This caused the tension in the *flexor* (F) to fall below the tendon lock threshold (G), which disabled the tendon spring. The unopposed tension produced a rapid extension of the tibia (H). Each chart corresponds to the output from a labeled element from Fig. 2.

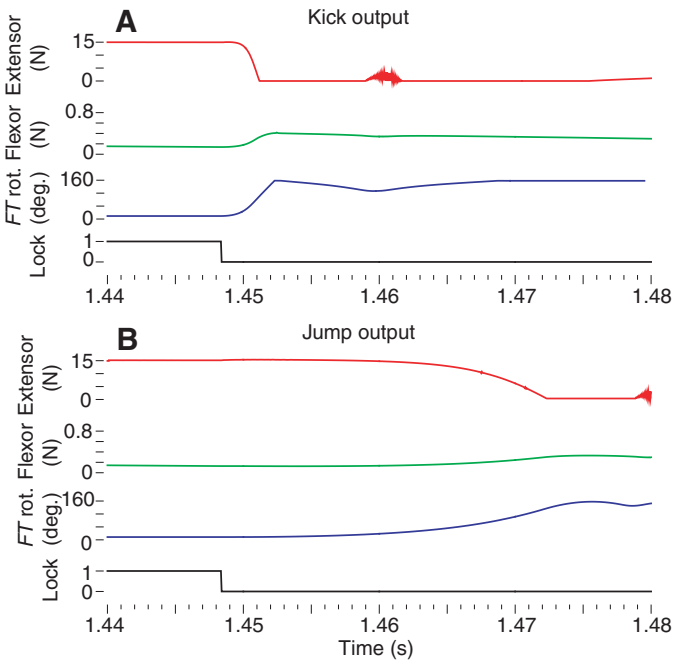

Fig. 4. Expanded view of *jump* or *kick* data. *Kick* data from Fig. 3 is expanded and compared with data from a *jump*. The output of the motor program was the same for both the *kick* and the *jump*, and so was omitted here. Each chart shows the tension in the *extensor* and *flexor* muscle of the *left metathoracic leg*, the rotation of the *femur–tibia* (*FT*) *joint* and the status of the *tendon lock*. (A) To produce a *kick*, the *tibia* began to rotate very rapidly after the *tendon lock* was disabled, and completed full extension in 4.1 ms. (B) The *jump* used the same motor program but the *leg* rotated more slowly because the *tibia* was loaded, and so reached its maximum value after 28.35 ms. The colored plot lines have the same colors as the corresponding lines for plots of the same variables in Fig. 3.

the *flexor muscles* that caused the left and right *tibiae* to become fully flexed (Fig. 3A,F). A train of current stimuli applied to the *FETi motorneurons* on both sides began the co-contraction phase (Fig. 3B,E). Each current stimulus evoked a corresponding spike in *FETi*. In addition to driving the *extensor muscle*, the *FETi* excited the *FlTi*s on the same side (Heitler, 1988) to enable the *flexor muscle* to keep the *tibia* flexed despite the mounting *extensor* tension. The *kick* was triggered by stimulation of the *FI* (Fig. 3D) and *M inhibitory neurons* (Fig. 3C) with an applied current for 80 ms, which caused them to fire at approximately 200 Hz. The *FI neuron* inhibited the *flexor muscle*, causing the *flexor* tension to decline rapidly. Simultaneously, the *M neuron* inhibited the *FlTi*s to remove the drive on the *flexor muscle*. Rapid inhibition of the *FlTi*s and the *flexor muscle* triggered the *kick* by reducing the *flexor* tension below the level needed to maintain the *tendon lock* (Fig. 3F,G) (Heitler and Burrows, 1977a; Pearson et al., 1980). With the *flexor tendon lock* disabled, the *tibia* began to extend very rapidly, completing extension in 4 ms, the same time course that was recorded with high-speed videography (Burrows and Morris, 2001).

To test the hypothesis that the same neural circuitry and motor program could produce both the kick and the jump, we used the model of the kick circuit and motor program to evoke a simulated jump. An expanded view of the data for both the *kick* and *jump* are shown in Fig. 4. Although the same motor program controlled both simulated behaviors, the unloaded *leg* extended in less than 5 ms to produce the *kick* (Fig. 4A) whereas the load imposed by the *body* caused the *leg* to extend much more gradually to produce the *jump* (Fig. 4B). Comparison of the simulated movements of the *locust* with a series of frames taken of a locust's jump (*S. americana*) by a high-speed camera operating at 500 frames s^{-1} (see Materials and methods; Fig. 5) shows that the simulation has captured the most salient features of the resulting jump behavior. In this, as in most of our recorded locust jumps, the animal's legs left the ground at about 30 ms after the start of the jump, and the head and thorax maintained their orientation during the 45 ms that the animal remained in view (Fig. 5, inset). Simulated *locust jumps* displayed most of these behaviors. The *locust* shown *jumping* in Fig. 5 displays the same series of *leg* movements at the same times as the locust shown in the inset, although its *body* has begun to rotate forward by the final frame of the simulation.

Published measurements of locust (*Schistocerca gregaria*) jump behavior (Table 1) provide benchmarks with which to compare the model *locust* jump behavior. Model *locust* jumps were performed with randomly seeded noise added to the *membrane potentials* of all of the model *neurons* and *muscles*, while all of the other model parameters were kept constant. Randomly seeded *membrane potential* noise ensured that the *locust* behaved slightly differently for each *jump* simulated under a given set of parameter values due solely to the randomness in the *neurons* and their effect on the biomechanics. This provided a method to measure the variance of the *behavior* when all of the other initial conditions were identical. By varying the *FETi* firing frequency *extensor tension* it was possible to encompass the entire range of behavioral data that was observed in the live animals. Several indicators of *jump* performance were

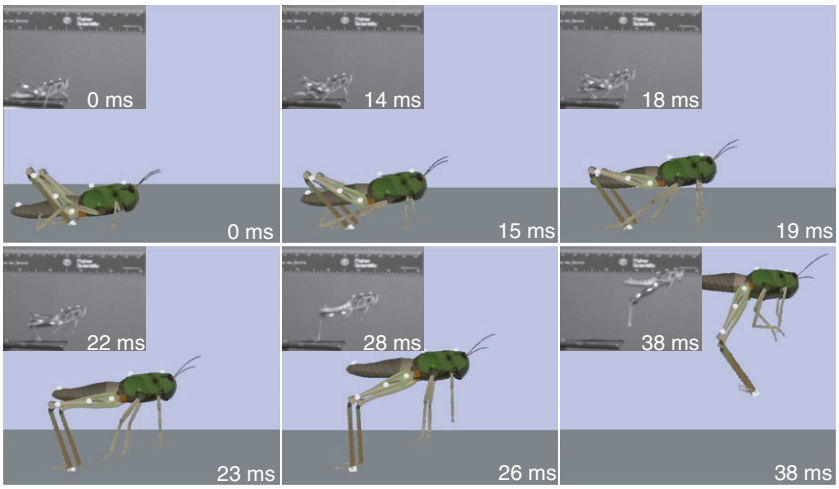

Fig. 5. Screenshots of the simulated and real locust jumping. Images of a real locust jump are in the insets. The simulated locust produces a *jump* very similar to those recorded from live locusts. Live locust images are sequential frames taken using a high-speed camera at 500 frames s^{-1}.

obtained and compared with the published benchmark values for live locusts (Table 1), and were found to be essentially the same. *FETi* frequencies between 44 Hz and 100 Hz produced *extensor* tensions from 9.4 N to 15 N that led to *jumps* between 46 cm and 120 cm long (Table 1; Fig. 6A circles, R^2=0.96). The simulations most closely matched the live data when the *FETi* frequency was set to 50 Hz, which evoked *extensor* tensions of 12 N and *jumps* 64 cm long. Energy for the *jump* also varied linearly and provided a very good match to the predicted distance for that energy level and take-off angle (Fig. 6B, R^2=0.98). These similarities demonstrate that the *jump* performance of the *locust* using the *kick* motor program closely matched that of the live locusts.

Role of the SLP

The contribution of the *SLP* to the *locust jump* was analyzed by comparing *jumps* made with the *SLP* intact with *jumps* made with it disabled. Without the *SLP*, the *jump* distance remained proportional to *extensor tension* but the slope of the regression line was reduced by 40% and the projected *X*-intercept (the minimal *extensor tension* needed to produce a *jump*) was greater (Fig. 6A squares, R^2=0.95). The difference in slope indicates that the *SLP* increases the effect of a change in *extensor* tension on the distance *jumped*. The difference in *X*-intercept provides a measurement of how energy storage by the *SLP* reduces the minimal *extensor* tension needed to make a *jump*. The difference between the two regression lines was used to determine the contribution of the *SLP* to *jump* distance for different *extensor tensions*. When the *SLP* was disabled the *jump* distance was reduced by 45% at 15 N and by 55% at 10 N. The peak power of the *jump* impulse when the *SLP* was intact was significantly higher than when the *SLP* was disabled (1.94±0.05 mW with, 1.10±0.04 mW without, $P<10^{-30}$; Fig. 7). A higher peak power also resulted in a significant increase in the total energy for the *jump* (15.3±0.4 mJ with, 8.58±0.4 mJ without, $P<10^{-30}$). In addition, when the *SLP* was disabled, the power ended significantly sooner than it did when the *SLP* was intact (24.7±0.3 ms with, 24.1±0.3 ms without, $P<10^{-10}$).

High-speed video of locust kicks have shown that the SLP does not unfurl until after the tibia has extended by more than 30 deg. (Burrows and Morris, 2001). To analyze this result through simulations, the locust kick was reproduced by the *locust*. Fig. 8A shows how the strain of the *SLP* and the *FT joint* rotation both vary with time during the *jump*. The filled black squares mark the values of the *SLP* strain at 1 ms intervals as they would be recorded by a high-speed video camera operating at 1000 frames s^{-1}, like those reported in fig. 3B of Burrows and Morris (Burrows and Morris, 2001). A significant unfurling of the *SLP* would first be detected 2 ms after start of the *jump* when photographed at 1000 frames s^{-1} (Fig. 8A,B, broken line *i*), when the *FT* rotation has reached 38.1 deg.

To understand what caused this delay it is useful to look at the *SLP* torque generated by the *SLP* force relative to the *extensor* attachment (Fig. 8B). The force of the *SLP* is applied at the *FT joint*, and so produced no direct torque around that *joint*, but it did produce a torque on the *tibia* around the *extensor attachment*. The *SLP* torque

Table 1. Comparison of real and simulated locust jump performances

Measurement	Units	Simulations			Animal
FETi frequency	Hz	44	50	100	0–100[‡]
Extensor tension	N	9.4±0.54	12±0.50	15±0.068	0–15*
Jump distance	cm	46±5.0	64±6.6	120±3.6	50–70*
Jump duration	ms	440±28	490±52	620±17	310–430*
Jump impulse duration	ms	32±1.3	28±0.78	25±0.19	25–30*
Peak jump velocity	m s^{-1}	2.2±0.10	2.6±0.12	3.6±0.054	2.2–3.2*
Peak jump acceleration	m s^{-2}	140±9.8	180±9.9	290±2.9	180*
Peak jump power	mW	0.57±0.050	0.92±0.068	1.9±0.034	0.75*
Jump energy	mJ	5.7±0.42	8.2±0.53	16±0.39	14*,[§]
Kick velocity	deg. m s^{-1}	39±2.1	45±1.5	62±0.30	54.5±1.3[†]
Kick duration	ms	6.2±0.36	5.4±0.16	4.1±0.022	3–6[†]

Comparison of key parameter values of the virtual locust jump with experimental values from live locusts. Different tensions in the *tibia extensor muscle* were obtained by varying the *FETi* frequency. Values are the averages and standard deviation obtained from 20 *jumps* or *kicks*. (*) (Bennet-Clark, 1975), (†) (Burrows and Morris, 2001), (‡) (Heitler and Burrows, 1977a), (§) Estimate at 15 N extensor tension.

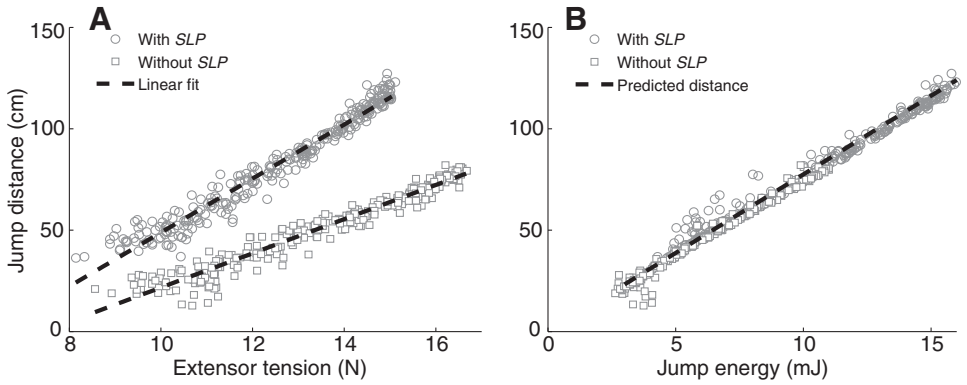

Fig. 6. *Jumping* performance. (A) *Jumps* were performed with and without the *semi-lunar process* (*SLP*) for a variety of different *extensor* tension values. *Extensor* tension was altered by varying the time between *FETi* spikes between 10 ms and 23 ms at 1 ms intervals. Twenty *jumps* were performed at each time interval. *Jump* distance varied linearly with *extensor* tension for both cases (R^2=0.96 with *SLP*, R^2=0.95 without *SLP*). Without the *SLP* the *jump* distance was reduced by 45% at 15 N, and this reduction increased to 55% at 10 N. (B) *Jump* distance also varied linearly with the *jump* energy, and matched the predicted *jump* distance (R^2=0.98). This is consistent with the hypothesized relationship between jump energy and distance (Bennet-Clark, 1975).

has a dual role: it acts to keep the *leg* flexed until *leg* extension begins, when it changes sign and accelerates *leg* extension. This sign reversal results from changes in the configuration of the *FT joint* during *leg* extension (Fig. 8; Movie 1 in supplementary material). The time needed for the sign reversal accounts for the delay.

The change in the sign of the *SLP* torque resulted from the change in position of the *extensor attachment* relative to the *SLP* force vector. At the beginning of the *kick*, with the *tibia* still flexed, the *SLP* force vector was directed above the *extensor attachment*, and so the *SLP* torque was negative, and acted to keep the *leg* flexed (Fig. 8B,C*i*). Moreover, the tension in the *extensor apodeme* kept the *SLP* strained. When the negative torque produced by the *flexor muscle* on the *FT joint* was removed by inhibition, the positive torque exerted by the *extensor muscle* on the *FT joint* began to extend the *leg*. Both the initial rotation of the *leg* and the shortening of the *extensor apodeme* reduced the force applied to the *SLP*, which began to reduce its strain (Fig. 8A, between *i* and *ii*). The *extensor attachment* was pulled through the *SLP* force vector, causing the negative (flexion) *SLP* torque to decrease and change to a positive (extension) torque (Fig. 8C *ii* and *iii*). At the time of this cross-over (Fig. 8A, broken line *ii*), the strain in the *SLP* had decreased by less than 10%. After the *SLP* torque became positive, it enhanced the *femoral–tibia joint* rotation, and the *extensor* tension could no longer maintain the *SLP* strain, which then rapidly decreased (Fig. 8A*iii*–C*iii*).

The negative *SLP* torque at the beginning of the *jump* assists the *flexor muscle* in maintaining the flexed position of the *tibia*. To determine the amount of assistance provided by the *SLP*, we compared the amount of *flexor* tension required to keep the *leg* flexed when the *SLP* spring was intact and when it was disabled. With the *SLP* spring intact, the *flexor muscle* held the *tibia* fully flexed until the *flexor* tension dropped to 0.26 N. When the *SLP* spring was disabled, the minimum *flexor* tension required to keep the *leg* from extending was 0.56 N. When the *SLP* spring was present it required 54% less tension in the *flexor muscle* to keep the *leg* from extending when the *tibia lock* was not active.

DISCUSSION

Motor program and jumping

The neural control and biomechanics of locust kicking have been well described because the kick can be evoked while the locust is dissected and restrained; thus, allowing simultaneous muscle electromyograms (EMGs) and intracellular recordings from central neurons. Although it is currently not possible to make these recordings in a jumping locust, the similarities between the kick and jump have led to the assumption that the same motor program may produce both behaviors. A computational neuromechanical model of the locust has allowed us to determine whether the neural circuit, the motor program and the biomechanical configuration of the locust legs are sufficient to account for the jump as well as the kick. Our results demonstrate that the kick motor program is capable of reproducing the full range of jump behaviors that have been described in the literature, and that the control of the key variable of extensor tension gives the locust the ability to alter important jump characteristics like jump distance and take-off velocity. Furthermore, we were also able to verify that the jump energy and take-off angle are good predictors of the final jump distance when the locust takes off with minimal tumbling. These results strongly support the hypothesis that the kick motor program is used for both kicking and jumping.

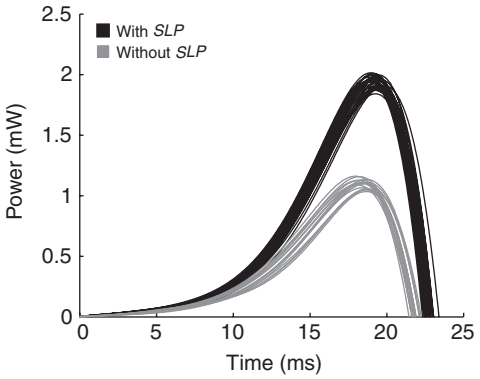

Fig. 7. *Jump* power with and without *semi-lunar process* (*SLP*). Only *extensor* tensions within 0.25 N of 15 N were used. *Jump* power with the *SLP* intact (black) and with the *SLP* disabled (gray). There is a significant difference in the magnitude of the peak power (1.94±0.05 mW with, 1.10±0.04 mW without, $P<10^{-30}$), the total energy during the *jump* impulse (15.3±0.4 mJ with, 8.58±0.4 mJ without, $P<10^{-30}$) and the duration of the impulse (24.7±0.3 ms with, 24.1±0.3 ms without, $P<10^{-10}$).

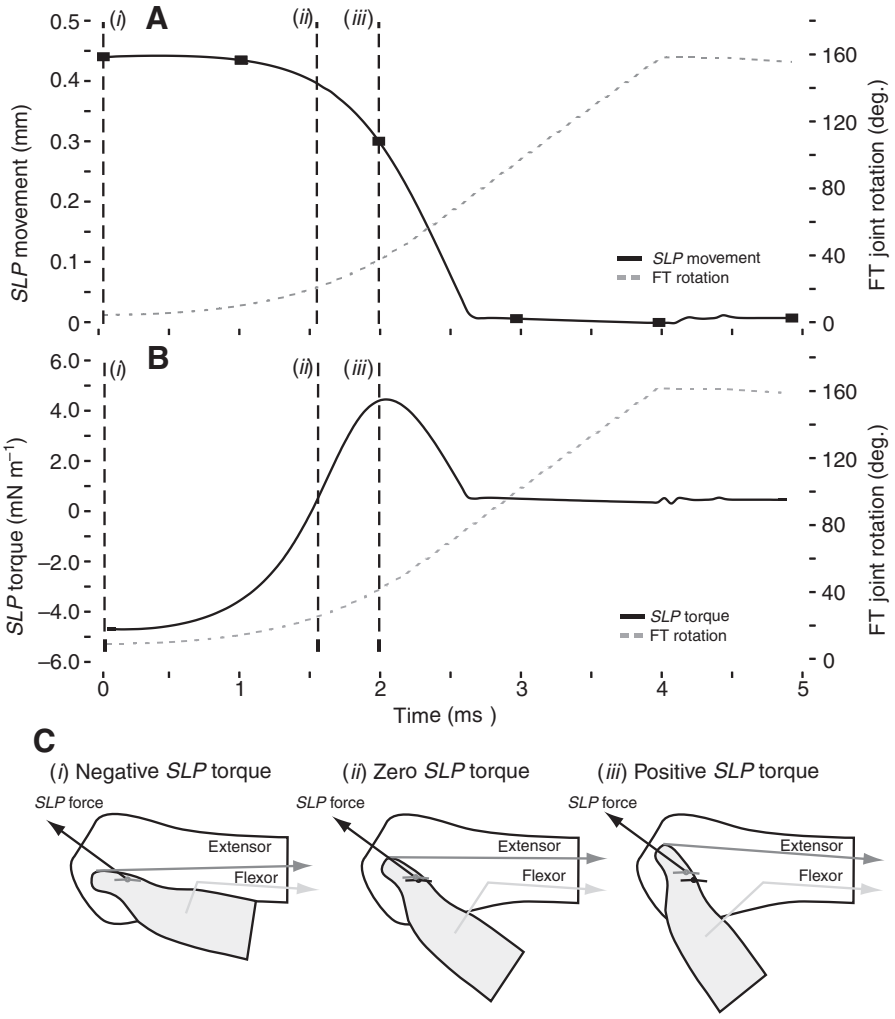

Fig. 8. *Semi-lunar process* (*SLP*) movement and torque during a *kick*. Prior to the *kick*, the *tibia* was flexed, the *extensor* tension was 15 N, *SLP* torque was –4.7 mN m^{-1}, and the *SLP* strain was nearly 4.5 mm. (A) The *femur–tibia* (*FT*) *joint* rotated with a maximum velocity of 63 deg. m s^{-1} and reached full extension of 160 deg. in 4 ms (broken gray line, right axis). The *SLP* strain decreased quickly during the *kick* (black line, left axis). The filled black squares represent the *SLP* positions at 1 ms time intervals when a high-speed camera at 1000 frames s^{-1} would take images [compare with fig. 3B of Burrows and Morris (Burrows and Morris, 2001)]. The beginning of the *kick* is shown with the broken vertical line (*i*). The first point where a noticeable decrease in the *SLP* would be visible at 1000 frames s^{-1} is shown with the broken vertical line (*iii*), which corresponds to a *FT* rotation of 38.12 deg. (B) *SLP* torque around the *extensor attachment* point (black line, left axis) was initially negative, which helped to maintain *leg* flexion. Significant *SLP* movement and *leg* extension occurred after the torque became positive, at broken vertical line (*ii*). (C) Negative *SLP* torque occurred when the force applied by the *SLP* caused torques that retarded *tibia* rotation (*i*), while positive torque enhanced *tibia* rotation. Positive torque only occurred after the *leg* had rotated enough to move the *extensor* attachment point to the opposite side of the *SLP* force vector (*iii*). Light gray hinge joint is the position of the *FT joint* at that time, while the black hinge is the position of the *FT joint* at the beginning of the *kick*. Figures in part C are for illustrative purposes only and are not drawn to scale.

Role of the SLP

The jump is an important behavior of locusts for both locomotion and escape from predators. The SLP is an evolutionary adaptation that has been thought to allow locusts to jump significantly farther than they could without it. However, because of the biomechanics of the metathoracic FT joint, direct tests of the effects of the SLP on jump performance of live locusts are difficult or impossible. The neuromechanical model of a locust presented here has allowed us to identify the contributions that the SLP makes to the jump. The simulations indicate that the SLP can help keep the leg flexed until the rotation of the tibia changes the sign of the SLP torque to favor extension. The SLP then approximately doubles the power of the jump.

The primary role of the flexor muscle of the metathorcic leg during jumping and kicking is to keep the tibia in a fully flexed position while co-contraction is occurring. The flexor muscle must be big enough to carry out this role but any excess volume devoted to the flexor muscle is wasteful and that volume would be better used by the extensor muscle to provide more power for the jump. We found that the *SLP* helps to maintain *leg* flexion during co-contraction, and so provides flexion torque that the *flexor muscle* would otherwise have to provide. When the *SLP spring* was disabled, any flexion torque that it generated was removed, and 54% more *flexor* tension was required to keep the *tibia* from extending. We suggest that the presence of the SLP enables the flexor muscle to be smaller than would be otherwise necessary, and that the savings in tibial volume may permit a relatively larger extensor muscle and more powerful jump.

High-speed video of locust kicking has shown that unfurling of the SLP is delayed until after the tibia had rotated by greater than 30 deg. (Burrows and Morris, 2001). The locust model helps to explain why there is such a delay in unfurling the SLP, and how this affects the jump abilities of locust. As shown in Fig. 8, the delay appears to depend on the movement of the *extensor tibiae* attachment point through the *SLP* force vector during the initial period of leg extension, changing an *SLP* torque that produced flexion to one that promotes *leg* extension. Finally, the simulations show that the *SLP* enables the *locust* to *jump* more than 45% farther than without it, depending on the force applied by the *extensor tibia*.

Storing energy by cuticle deformation or strain in apodemes are common methods of overcoming the limitations of skeletal muscle that are required for arthropods to make quick movements like jumping and snapping (Gronenberg, 1996). Some of these animals have evolved elaborate specializations to allow them to perform these rapid movements. The rabbit flea *Spilopsyllus cuniculus* stores energy for its jump in a resilin pad in the internal skeleton of its thorax but is released when the force vector passes over the leg joint and is redirected from leg flexion to leg extension, like the locust SLP (Bennet-Clark and Lucey, 1967). The froghopper *Philaenus spumarius* stores energy for the jump by bending a bow-like cuticle formation in the pleural arch. A friction-locking system

prevents the legs from moving until tension in the depressors exceeds the holding force of the lock (Burrows, 2003; Burrows, 2006; Burrows et al., 2008). Both the trap-jaw ant *Odontomachus bauri* and the snapping shrimp *Alpheus californiensis* store energy for the rapid closing of their mandible or claw in the apodeme of the muscle and by deformation of the cuticle of the exoskeleton (Gronenberg, 1995a; Gronenberg, 1995b; Ritzmann, 1973). The shrimp *Alpheus heterochelis* has a mechanism similar to the flea where the locking of the closer occurs when the force vector is brought above the pivot point, and release occurs when an accessory closer muscle pulls it back down to generate a large closing torque (Ritzmann, 1974).

While all of these mechanisms are similar, there is a difference that appears to be unique to the SLP mechanism of the locust. Energy from the jump primarily comes from the apodeme of the extensor and the SLP. In the locust the SLP and apodeme produce forces that act at different sites and in different directions, and this is a key feature for causing the delay in unfurling the SLP. The energy storage mechanisms used by the flea (Bennet-Clark and Lucey, 1967) and the shrimp (Ritzmann, 1974) both have similarities and differences with the system described here. They are similar in that the movement of the force vector causes a reversal in the direction of a torque. In the shrimp this occurs when the closer muscle is pulled from one side of the joint to the other. In the *locust* this happens when the *extensor apodeme* is pulled through the *SLP* force vector. The difference is because the shrimp and flea use a small accessory muscle to pull the main contractile muscle over a joint, whereas in the locust it is the biomechanics of the movement of the joint that causes the *SLP* torque reversal.

Conclusion

This work demonstrates the utility of neuromechanical simulation for analysis of the interaction of neural mechanisms of control with biomechanical processes that mediate and constrain the animal's movement. Neuromechanical simulation enables the operation of neural circuits that have been described in dissected, restrained and anesthetized animals to be understood in something like their natural context, where the consequences of their activity for movement become readily apparent.

One area of future study that these simulations identified is the role of tumbling during the jump. The take-off angle can be controlled by the orientation of the rear legs (Sutton and Burrows, 2008). We have noted in simulations that a change in orientation can produce a take-off angle where the thrust vector is not aligned with the *locust's* COM. On those occasions, the *locust* displayed *tumbling behavior* during the *jump* that was qualitatively different from that of live animals jumping with similar take-off angles. We believe that locusts may have several mechanisms for preventing unwanted tumbling at different take-off angles, including the setting the initial body elevation, changing the body posture during take-off and controlling the transfer of momentum between the legs and body. The *locust* model may prove useful in studying those mechanisms and their importance.

A second area is the role of reafference in the control of the jump. The direction and distance of a jump are controlled by the initial posture of the animal and the tension in the extensor tendon (Santer et al., 2005; Sutton and Burrows, 2008). Several sets of proprioceptors that provide sensory information useful for this control have been identified, and the roles that some play during kicking have been described (Burrows and Pfluger, 1988; Heitler, 1977; Heitler, 1995). However, it is unclear how the reafferent responses or their uses might be modified for jumping, when both the load conditions and the constraints imposed by the initial setup are different. Given the great difficulties in addressing these questions experimentally, simulations of reafferent responses under the closed-loop conditions that lead to the jump may prove helpful.

ACKNOWLEDGEMENTS

We wish to acknowledge support for this work from National Science Foundation research grant 0641326 to DHE; from a Brains and Behavior Seed Grant from Georgia State University, from the Brains and Behavior Fellowship Program at Georgia State University, and from National Institutes of Health exploratory grant GM065762. We would also like to thank Dr Karen Thompson of Agnes Scott College for supplying us with locusts for testing, and for instructing us on their maintenance and care. Deposited in PMC for release after 12 months.

REFERENCES

Bennet-Clark, H. C. (1975). The energetics of the jump of the locust *Schistocerca gregaria*. *J. Exp. Biol.* **63**, 53-83.
Bennet-Clark, H. C. and Lucey, E. C. (1967). The jump of the flea: a study of the energetics and a model of the mechanism. *J. Exp. Biol.* **47**, 59-67.
Burrows, M. (1995). Motor patterns during kicking movements in the locust. *J. Comp. Physiol. A* **176**, 289-305.
Burrows, M. (1996). *The Neurobiology of an Insect Brain*. Oxford: Oxford University Press.
Burrows, M. (2003). Biomechanics: froghopper insects leap to new heights. *Nature* **424**, 509.
Burrows, M. (2006). Morphology and action of the hind leg joints controlling jumping in froghopper insects. *J. Exp. Biol.* **209**, 4622-4637.
Burrows, M. and Morris, G. (2001). The kinematics and neural control of high-speed kicking movements in the locust. *J. Exp. Biol.* **204**, 3471-3481.
Burrows, M. and Pfluger, H. J. (1988). Positive feedback loops from proprioceptors involved in leg movements of the locust. *J. Comp. Physiol.* **163A**, 425-440.
Burrows, M., Shaw, S. R. and Sutton, G. P. (2008). Resilin and chitinous cuticle form a composite structure for energy storage in jumping by froghopper insects. *BMC Biol.* **6**, 41.
Gronenberg, W. (1995a). The fast mandible strike in the trap-jaw ant *Odontomachus*. I. Temporal properties and morphological characteristics. *J. Comp. Physiol. A.* **176**, 391-398.
Gronenberg, W. (1995b). The fast mandible strike in the trap-jaw ant *Odontomachus*. II. Motor control. *J. Comp. Physiol. A.* **176**, 399-408.
Gronenberg, W. (1996). Fast actions in small animals: springs and click mechanisms. *J. Comp. Physiol. A.* **178**, 727-734.
Heitler, W. (1974). The locust jump. Specialisations of the metathoracic femoral-tibia joint *J. Comp. Physiol.* **89**, 93-104.
Heitler, W. (1977). The locust jump. III. Structural specializations of the metathoracic tibiae. *J. Exp. Biol.* **67**, 29-36.
Heitler, W. (1988). The role of fast extensor motor activity in the locust kick reconsidered. *J. Exp. Biol.* **136**, 289-309.
Heitler, W. J. (1995). Quasi-reversible photo-axotomy used to investigate the role of extensor muscle tension in controlling the kick motor programme of grasshoppers. *Eur. J. Neurosci.* **7**, 981-992.
Heitler, W. J. and Burrows, M. (1977a). The locust jump. I. The motor programme. *J. Exp. Biol.* **66**, 203-219.
Heitler, W. J. and Burrows, M. (1977b). The locust jump. II. Neural circuits of the motor programme. *J. Exp. Biol.* **66**, 221-241.
Hill, A. V. (1970). *First and Last Experiments in Muscle Mechanics*. Cambridge: Cambridge University Press.
MacGregor, R. and Lewis, E. (1977). *Neural Modeling: Electrical Signal Processing in the Nervous System*. New York: Plenum Press.
McMahon, T. A. (1984). *Muscles, Reflexes, and Locomotion*. New Jersey: Princeton University Press.
Pearson, K., Ekeberg, O. and Buschges, A. (2006). Assessing sensory function in locomotor systems using neuro-mechanical simulations. *Trends Neurosci.* **29**, 625-631.
Pearson, K. G., Heitler, W. J. and Steeves, J. D. (1980). Triggering of locust jump by multimodal inhibitory interneurons. *J. Neurophysiol.* **43**, 257-278.
Ritzmann, R. (1973). Snapping behavior of the shrimp *Alpheus californiensis*. *Science* **181**, 459-460.
Ritzmann, R. (1974). Mechanisms for the snapping behavior of two alpheid shrimp, *Alpheus californiensis* and *Alpheus heterochelis*. *J. Comp. Physiol.* **95**, 217-236.
Santer, R. D., Yamawaki, Y., Rind, F. C. and Simmons, P. J. (2005). Motor activity and trajectory control during escape jumping in the locust *Locusta migratoria*. *J. Comp. Physiol. A Neuroethol. Sens. Neural Behav. Physiol.* **191**, 965-975.
Shadmehr, R. and Wise, S. (2005a). *Computational Neurobiology of Reaching and Pointing: A Foundation for Motor Learning*. Cambridge, MA: MIT Press.
Shadmehr, R. and Wise, S. (2005b). A simple muscle model. (Supplement to Shadmehr and Wise, 2005a). Online at http://www.shadmehrlab.org/book/musclemodel.pdf.
Sutton, G. P. and Burrows, M. (2008). The mechanics of elevation control in locust jumping. *J. Comp. Physiol. A Neuroethol. Sens. Neural Behav. Physiol.* **194**, 557-563.